Three-phase Transformer Model and Parameter Estimation for ATP

Sung-Don Cho*

Abstract - The purpose of this paper is to develop an improved three-phase transformer model for ATP and parameter estimation methods that can efficiently utilize the limited available information such as factory test reports. In this paper, improved topologically-correct duality-based models are developed for three-phase autotransformers having shell-form cores. The problem in the implementation of detailed models is the lack of complete and reliable data. Therefore, parameter estimation methods are developed to determine the parameters of a given model in cases where available information is incomplete. The transformer nameplate data is required and relative physical dimensions of the core are estimated. The models include a separate representation of each segment of the core, including hysteresis of the core, λ-i saturation characteristic and core loss.

Keywords: ATP, Autotransformer, Duality, EMTP, Shell-form, Optimization, Parameter estimation

1. Introduction

ATP offers two different transformer models. STC is a built-in model. It is limited to single-phase or three-phase banks made up of single-phase units. No mutual coupling between the phases can be taken into account. In addition, it is not possible to represent the differences between the positive and the zero sequence paths [1].

BCTRAN is the supporting routine of the EMTP program, which creates an impedance or admittance matrix representation of the transformer, without taking into account the saturable core effects, from transformer ratings and factory test data. In this model, it is possible to represent the differences between the positive and the zero sequence paths. However, unequal phase reluctances and nonlinear interactions between limbs of the core cannot be taken into account [1].

Topologically-correct equivalent circuit models can be derived from magnetic circuit models using the principle of duality. This type of model includes the effects of saturation in each individual leg of the core as well as leakage effects. The equivalent circuits resulting from duality transformations are topologically correct lumped-parameter representations [2]. Duality-derived models can be implemented with standard EMTP elements. However, practical application of this model for a three-phase transformer has been hampered by some difficulty in obtaining the required model parameters.

* Plant Engineering Team, Samsung Corporation, Korea.
(sungdon.cho@samsung.com)
Received: December 1, 2005 ; Accepted: April 12, 2006

2. Three-phase Autotransformer Data

The use of an autotransformer makes it possible for a high power rating to be constructed as a single unit three-phase transformer. To develop a model for a three-phase autotransformer, transformer physical design information and characteristic data are needed. However, it is most unusual to have a case where complete physical design information and dimensions are available. Often, all the information that we have is what is on the nameplate, or what is gleaned from the basic factory tests, if those are obtainable.

Typical transformer factory test reports available from manufacturers consist of data much like what is presented in Table 1. The available data are kW losses and true RMS exciting current at 100% and 110% of the rated voltage. There is no information on transformer core dimension, core material, etc. It should be noted that the "RMS exciting current" taken from factory tests is actually the average of the three measured RMS phase currents.

Table 1. Transformer Test Data

345000 Grd.Y/118000 Grd.Y/13800 Delta, 3-phase auto-transformer @OA/FOA/FOA H-296/394/490MVA, X-296/394/490MVA, Y-77/103/128MVA		
Open-Circuit Test	Exciting Current	No Load Loss
	0.76%@100%V	297.6kW@100%V
	1.71%@110%V	402.24kW@110%V
Short-Circuit Test	Impedance	Load Loss
H-X	6.21% @296MVA	378.94kW @296MVA
H-Y	55.9% @296MVA	258.76kW @77MVA
X-Y	42.1% @296MVA	237.68kW @77MVA

3. Duality-Based Model

Detailed models incorporating core nonlinearities can be derived by applying the principle of duality on topology-based magnetic models. This approach is very useful for creating models accurate enough for low-frequency transients. The mesh and node equations of the magnetic circuit are the duals of the electrical equivalent's node and mesh equations respectively.

The structure of a three-phase shell-form transformer is shown in Fig. 1. The fluxes in the core are $\Phi_1 = \Phi_A/2$, $\Phi_2 = \Phi_B/2$, $\Phi_3 = \Phi_C/2$, $\Phi_4 = \Phi_A - \Phi_B$, $\Phi_5 = \Phi_B - \Phi_C$.

The lumped magnetic circuit representing the three-phase shell-form transformer is presented in Fig. 2. The windings are represented by MMF sources. Reluctances $\Re_x$, $\Re_o$, $\Re_m$ signify the portions of the core with a cross section that is about 50% that of the core inside the windings. Reluctances $\Re_x$, $\Re_o$, $\Re_m$ represent the parallel combinations of two reluctances for upper and lower core sections (the core structure in Fig. 1 was horizontally folded due to symmetry, simplifying the resulting lumped magnetic circuit). These portions of the core thus have the same conditions of saturation as the core inside the windings.

A shell-form transformer is designed so that the middle limbs ("$\Re_y$") can carry two fluxes, permitting economy in the core construction and lower losses. The mean turn length is usually longer than for a comparable core-form design, while the iron path is shorter.

Fig. 3 indicates the equivalent electric circuit for the shell-form transformer.

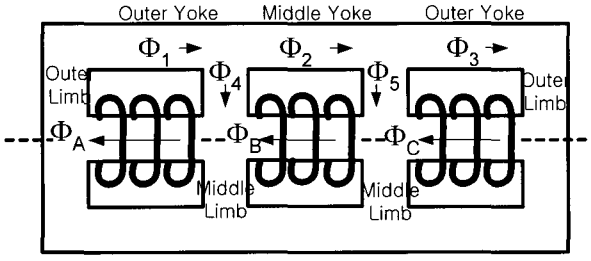

Fig. 1. Shell-form Transformer Structure

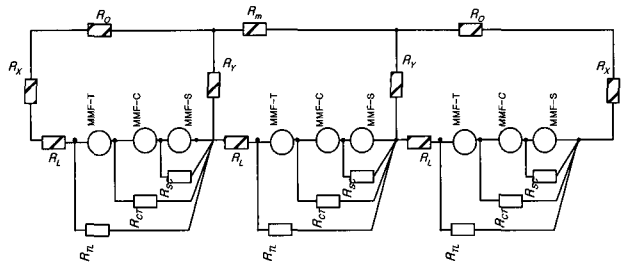

Fig. 2. Magnetic Circuit for Shell-form Transformer

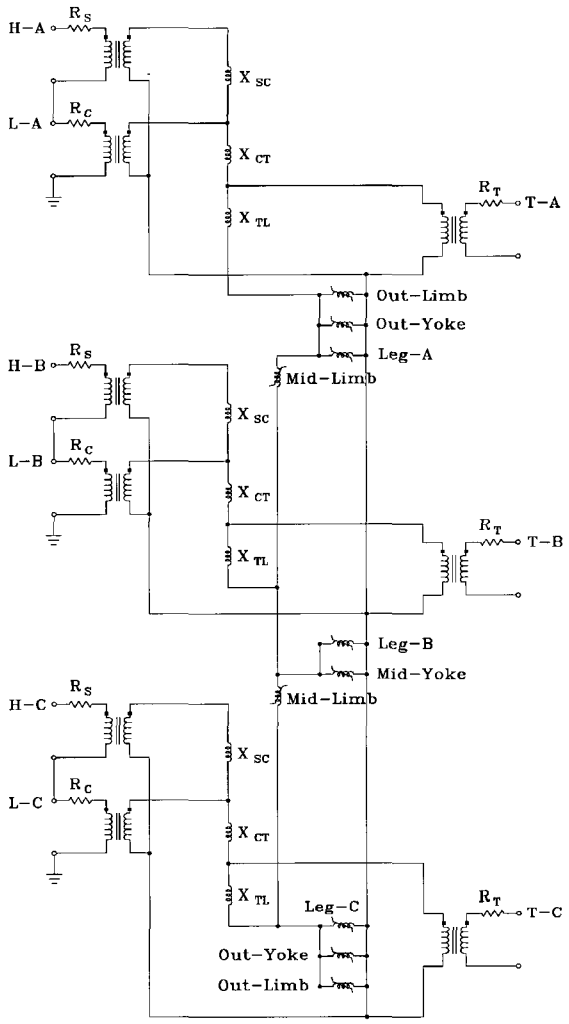

Fig. 3. Equivalent Electric Circuit for Sell-form Transformer

4. Parameter Estimation for Transformer Model

4.1 Leakage Inductance

The leakage reactances X_{SC} and X_{CT} in Fig. 3 are calculated from the test data and scaled to per unit based on the voltage across each winding. The leakage reactance X_{TL} is related to the leakage channel between the tertiary winding and the core.

Parameter $k=a_1/a_2$ is typically used with a_1, which is the width of the leakage channel between the tertiary winding and the core and a_2 is the width of the leakage channel between the T-winding and the C-winding. If the leakage reactance X_{CT} for a three winding transformer are given then the leakage reactance X_{TL} to the core winding are assumed to be $X_{TL}=k*X_{CT}$ The leakage reactances according to the H-X-Y sequence are now sorted according to the S-C-T sequence and the leakage reactance X_{TL} related to the artificial core winding is established.

4.2 Core Saturation

For a shell-form transformer, cross-sectional area ratios in Fig. 4 were assumed on the basis that the flux density is the same for all paths. The portions of the core thus have the same conditions of saturation as the core inside the windings. Lengths were chosen on the basis that since most coil types are pancake type, then legs and yokes are longer than the limbs. Reluctances $\Re_4 \sim \Re_{10}$ in Fig. 5 represent the parallel combinations of two reluctances for upper and lower core sections.

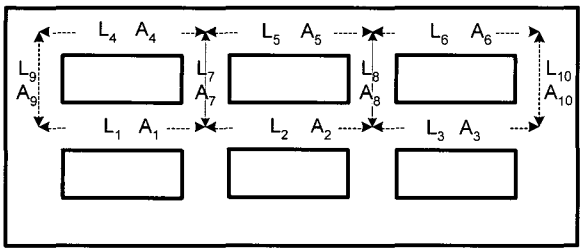

Notation: A: Area, L: Length, Typical Area ratio: $A_1 \sim A_3=1$, $A_4 \sim A_6=0.5$, $A_7 \sim A_8=0.87$, $A_9 \sim A_{10}=0.5$, Typical Length ratio: $L_1 \sim L_6=1$, $L_7 \sim L_{10}=0.67$

Fig. 4. Dimension of Shell-form Transformer

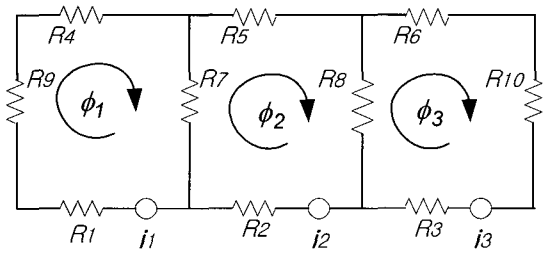

Fig. 5. Magnetic Equivalent Circuit

$$i_1 = \phi_1(R_1+R_4+R_9)+R_7(\phi_1-\phi_2) \quad (1)$$

$$i_2 = \phi_2(R_2+R_5)+R_7(\phi_2-\phi_1)+R_8(\phi_2-\phi_3) \quad (2)$$

$$i_3 = \phi_3(R_3+R_6+R_{10})+R_8(\phi_3-\phi_2) \quad (3)$$

where, $R_1=L_1/(\mu_1 A_1)$, $\mu_1=f(\phi_1/A_1)$, $R_2=L_2/(\mu_2 A_2)$, $\mu_2=f(\phi_2/A_2)$, $R_3=L_3/(\mu_3 A_3)$, $\mu_3=f(\phi_3/A_3)$, $R_4=L_4/(2\mu_4 A_4)$, $\mu_4=f(\phi_1/2/A_4)$, $R_5=L_5/(2\mu_5 A_5)$, $\mu_5=f(\phi_2/2/A_5)$, $R_6=L_6/(2\mu_6 A_6)$, $\mu_6=f(\phi_3/2/A_6)$, $R_7=L_7/(2\mu_7 A_7)$, $\mu_7=f((\phi_1-\phi_2)/2/A_7)$, $R_8=L_8/(2\mu_8 A_8)$, $\mu_8=f((\phi_2-\phi_3)/2/A_8)$, $R_9=L_9/(2\mu_9 A_9)$, $\mu_9=f(\phi_1/2/A_9)$, $R_{10}=L_{10}/(2\mu_{10} A_{10})$, $\mu_{10}=f(\phi_3/2/A_{10})$

In order to estimate the core saturation, variables are classified as known and unknown:

Known values: *$\phi_1=v_1/(\omega N)$, $\phi_2=v_2/(\omega N)$, $\phi_3=v_3/(\omega N)$ v=peak-voltage for each phase, $\omega=2\pi f$, N = number of turn*

Magnetizing Current: $I_{rms,AVG}=(I_{1,rms}+I_{2,rms}+I_{3,rms})/3$

Core dimensions or ratios (A and L)

Unknown values: *a, b for* $\mu = \frac{B}{H} = \frac{(1-b\cdot B)}{a}$ (4)

If the core dimension ratios and average RMS magnetizing currents at 100% and 110% voltages are given, some optimization techinique can be used to estimate the a and b coefficients for the B-H Frolich Equation (4) [3], [6].

The optimization performed is as follows:

$$\phi_1(k)=v_1/(\omega N)\times\sin(\pi\cdot k/40) \text{ and } \phi_2(k)=v_2/(\omega N)\times\sin(\pi\cdot k/40-2\pi/3)$$

$$B_1(k)=B_4(k)=B_9(k)=\phi_1(k)/A_1 \text{ and } B_7(k)=(\phi_1(k)-\phi_2(k))/2/A_7)$$

$$\mu_1(k)=\frac{1-b\cdot B_1(k)}{a} \text{ and } \mu_7(k)=\frac{1-b\cdot B_7(k)}{a}$$

$$R_1(k)=L_1/(\mu_1(k)\cdot A_1) \text{ and } R_7(k)=L_7/(\mu_7(k)\cdot A_7)$$

$$i_1(k)=\phi_1(k)\cdot(R_1(k)+R_4(k)+R_9(k))+R_7(k)\cdot(\phi_1(k)-\phi_2(k))$$

$$I_{1,RMS}=\sqrt{\frac{\sum_{k=1}^{40}(i_1(k))^2}{40}} \text{ and } I_{RMS,AVG}=(I_{1,RMS}+I_{2,RMS}+I_{3,RMS})/3$$

Minimize $f(a,b)=$

$$\left[\text{Measured } I_{AVG,RMS}@100\%V - \text{Calculated } I_{AVG,RMS}@100\%V\right]^2 + \left[\text{Measured } I_{AVG,RMS}@110\%V - \text{Calculated } I_{AVG,RMS}@110\%V\right]^2$$

Subject to inequality constraints $0 < a$ and $0 < b < 1$

From the optimization technique, the results are a=3.7651, and b=0.5651. Fig. 6 shows the obtained B-H curve. The calculated RMS currents for the three phases are [99.9829, 107.5387, 107.5386]A at 100% voltage. The calculated average RMS current is 105.02A and the difference from the test report is only 7.9357×10^{-5}A. The calculated RMS currents for the three phases are [215.8171, 228.2594, 228.2594]A at 110% voltage. The calculated average RMS current is 224.11A and the difference from the test report is 3.7518×10^{-5}A. Fig. 7 shows the λ-i curve for each core section of the example transformer. Fig. 8 presents the simulated current waveforms of lines at 100% voltage.

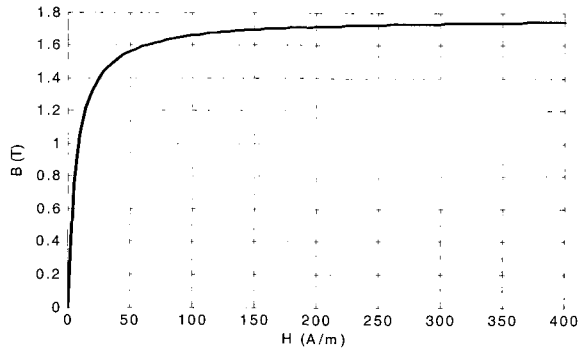

Fig. 6. B-H for Each Section

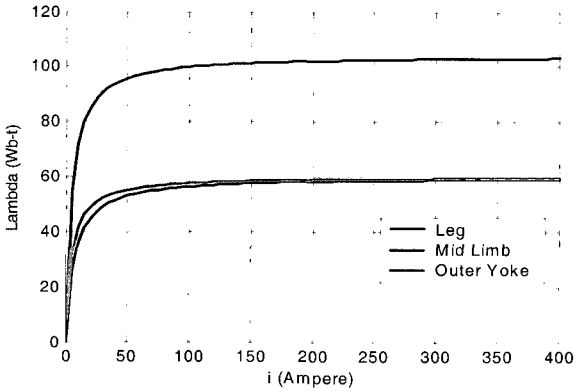

Fig. 7. λ-i Magnetization Curves for Each Section

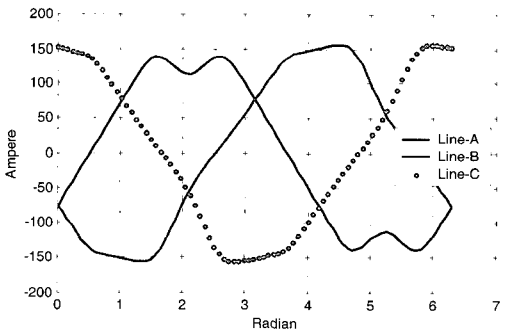

Fig. 8. Current Waveforms for Each Line at 100% Voltage

4.3 Core Loss Model

The modeling of eddy currents and hysteresis has been approximate and difficult, because of the lack of information. In the approach developed here, parameters for the transformer model are estimated using basic transformer test data and optimization techniques.

For the detailed model, separation of the core losses is:

P_C(core loss) = P_H(hysteresis loss) +P_E(eddy current loss)

From test data, average core losses at 100% voltage and 110% voltage are given as [297600, 402240]W at λ = [51.77, 56.95]Wb-t.

The calculated average core loss should be:

$$\sum_{n=1}^{10} P_n(B_n)\cdot A_n\cdot L_n = \sum_{n=1}^{10}\frac{a\cdot B_n}{1-b\cdot B_n}\cdot A_n\cdot L_n \tag{5}$$

The optimization performed is as follows:

Minimize f(a,b)=

$$\left[P@100\%V-\sum_{n=1}^{10}\frac{a\cdot B_n}{1-b\cdot B_n}\cdot A_n\cdot L_n\right]^2+\left[P@110\%V-\sum_{n=1}^{10}\frac{a\cdot B_n}{1-b\cdot B_n}\cdot A_n\cdot L_n\right]^2$$

Subject to inequality constraints 0 < a and 0 < b < 1

Thus, a= 7071.8 and b =0.4272 are calculated for the core saturation curve by using the optimization technique. In this case, there is only a minor difference [0.0152 0.0112] W between the given core loss and the calculated core loss. If the ratio(α) of P_H to total core loss and the ratio (β) of P_E to total core loss given to define the frequency-dependent effects of core loss, the equivalent resistance (R_E) for P_E is:

$$R_E = V^2/(P_E\cdot A\cdot L) = (V@B)^2/[\beta\cdot(P_C@B)\cdot(A\cdot L)]\ (\Omega) \tag{6}$$

In [6], the equation for DC hysteresis loss was given as Equation (10). From the core loss separation, "aa" and "bb" are obtained.

$$P_H(B_{MAX}) = P_C(B_{MAX}) - P_E(B_{MAX}) = \frac{aa\cdot B_{MAX}}{1-bb\cdot B_{MAX}} \tag{7}$$

Fig. 9 shows each core loss curve for the shell-form transformer.

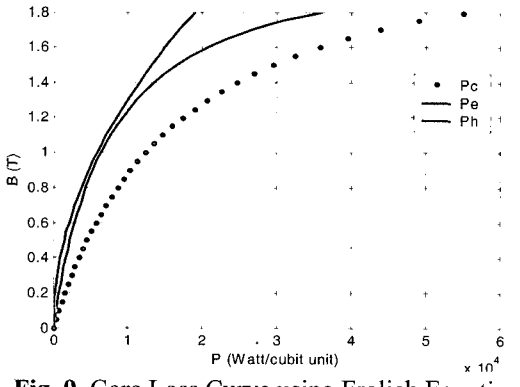

Fig. 9. Core Loss Curve using Frolich Equation

The right displacement in the hysteresis loop is linear and the left displacement is nonlinear in [6]. At zero flux, both displacements must be the same and this is a coercive force (H_C). The coercive force at each loop should be determined to meet the power loss P_H at the B_{max} for each loop.

The displacements at each loop are shown in Figure 10.

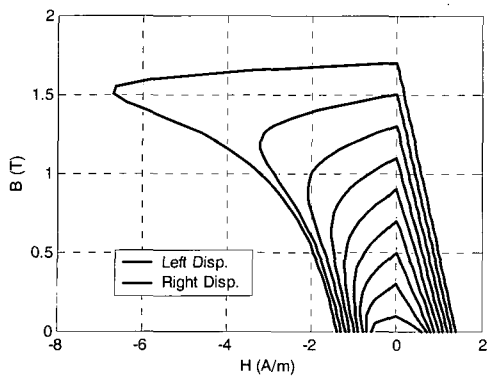

Fig. 10. Left and Right Displacements of Hysteresis Current

5. Conclusion

The overall transformer model for ATP implementation is shown in Fig. 3. Fig. 11 displays the DC hysteresis loop modeled using a Type-60 current source controlled by TACS. Fig. 12 illustrates the current of the eddy current loss and the resistive hysteresis current. Fig. 13 shows the magnetizing current modeled with a Type-93 nonlinear inductance. Fig. 14 and 15 show the line-current and winding-current waveforms.

To verify the transformer model developed using TACS, results from simulated open circuit tests were compared to the transformer test report. After all models were implemented and run with ATP, the results of open-circuit and short-circuit simulations are very close to the test report.

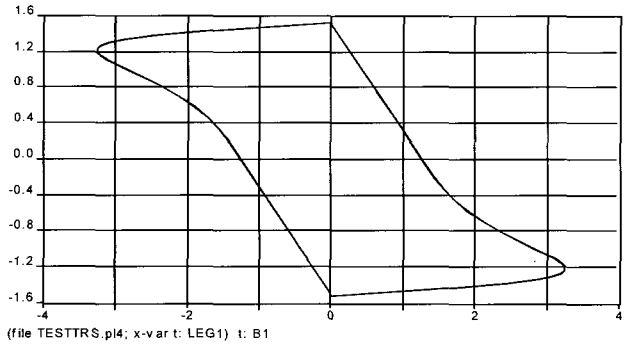

Fig. 11. DC Hysteresis Loop Generated by ATP

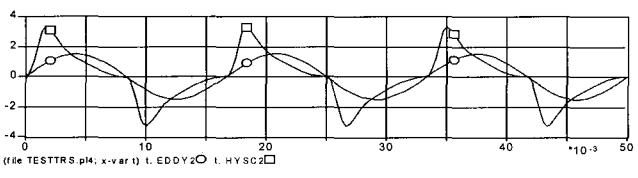

o: i_E : i_H

Fig. 12. Eddy Current(i_E) and Hysteresis Current(i_H) Waveforms at 100%V

The simulated results using the model developed here are reasonable and more correct than those of the BCTRAN-based model. Simulation accuracy is dependent on the accuracy of the equipment model and its parameters. This work is significant in that it advances existing parameter estimation methods in cases where the available data and measurements are incomplete. Theoretical results obtained from this work provide a sound foundation for the development of transformer parameter estimation methods using engineering optimization. To further refine and develop the models and transformer parameter estimation methods developed here, iterative full-scale laboratory tests using high-voltage and high-power three-phase transformers would be helpful.

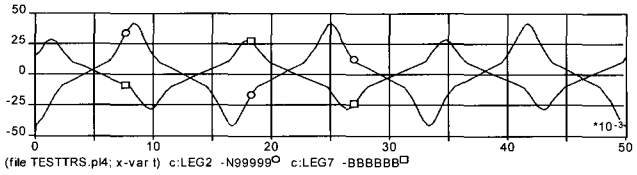

o: Leg-1 : Mid Limb A-B at 100%V

Fig. 13. Mangnetizing Current Waveforms of Leg 2 and Mid Limb A-B (Leg-7)

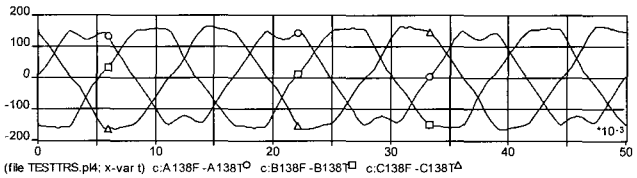

o: Line-A : Line-B Δ: Line-C

Fig. 14. Line Current Waveforms for Tertiary at 100% V

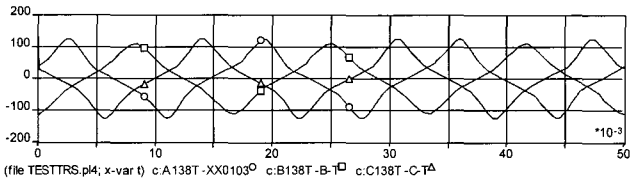

o: Phase-A : Phase-B Δ: Phase-C

Fig. 15. Winding Current Waveforms for Tertiary at 100% V

References

[1] H.W. Dommel, EMTP Theory Book, *Bonneville Power Administration, Portland, USA, August 1986.*

[2] G.R. Slemon, "Equivalent Circuits for Transformers and Machines Including Non-Linear Effects", Proceedings Institution of Electrical Engineers, Vol. 100, Part IV, 1953, pp. 129-143.

[3] Working Group C-5 of the Systems Protection Subcommittee, "*Mathematical models for current,*

voltage, and coupling capacitor voltage transformers", IEEE Transactions on Power Delivery, Vol. 15 Issue: 1, Jan. 2000, pp. 62 –72.

[4] Armco Catalog, "Oriented and TRAN-COR H Electrical Steels", 10th Edition, Jan. 1986.

[5] M. J. Heathcote, The J&P Transformer Book - 12th Edition, *Newnes Ltd., 1998.*

[6] Sung Don Cho, *"Transformer Core Model and Parameter Estimation for ATP"*, KIEE International Transactions on Power Engineering, vol. 5-A, no. 4, 2005.

Sung-Don Cho

He received his Ph.D. degree from Michigan Tech University in 2002. His research interests are transient analysis, EMTP and ATP application.